Identification of inelastic processes in 4.0-keV H_2^+-He collisions using L_α-photon–particle coincidence techniques

D. Calabrese, L. M. Wiese, O. Yenen, and D. H. Jaecks
Behlen Laboratory of Physics, University of Nebraska, Lincoln, Nebraska 68588-0111
(Received 2 August 1994)

The laboratory energy distribution of protons in coincidence with L_α photons produced in collision-induced dissociation of 4.0-keV H_2^+ on He targets has been measured for protons that are collected along the incident-beam direction. An approximate energy distribution of proton–L_α-photon pairs in the projectile frame is obtained by transforming the measured laboratory distribution. The transformed results reveal that the dominant processes for production of near-zero energy projectile frame protons are the $1s\sigma_g$ to $2p\pi_u$ and $3d\sigma_g$ transition at 2.5–3 times the equilibrium separation of H_2^+. This transformation technique provides a simple method of identifying inelastic processes from the convoluted laboratory energy distributions of the fragments produced in the dissociative excitation of the H_2^+ molecule.

PACS number(s): 34.50.Gb

I. INTRODUCTION

An outstanding problem in the study of inelastic low kilo-electron-volt atom-molecule collisions is the identification of the excited molecular states that produce fragment particles of various projectile frame energies upon excitation and dissociation of the parent molecule. This identification is important if one hopes to determine the mechanisms that produce the excited states of a molecule in atom-molecule collisions. In general, there are no "rules of thumb" or analogous Fano-Lichten rules [1] that describe molecular excitation in inelastic atom-molecule collisions, as in the case of ion-atom collisions. Although, there have been numerous investigations of simple atom-molecule systems such as H_2^+-He, identification and thus understanding of the inelastic processes involved are still not well understood.

In this paper, we add a piece to this puzzle of identifying and understanding inelastic processes by reporting the measurement of the laboratory energy distribution of protons in coincidence with L_α photons resulting from the dissociation of $(H_2^+)^*$ produced in 4.0-keV H_2^+-He collisions. Coincidence measurements between protons and polarized L_α photons produced in atom-molecule collisions were originally carried out by Jaecks *et al.* [2] for 3.22-keV H_2^+-He collisions. The measurement of this particular process allows one to probe a specific portion of the characteristic total proton laboratory energy spectrum, shown in Fig. 1, that is related to the production of $H(2p)$ [3]. Specifically, we extract information about the processes that produce near-zero energy projectile frame protons upon dissociation of the excited H_2^+ molecule. The measurements are performed for the case in which the proton is produced and detected along the incident-beam direction. From this measurement, we estimate the projectile frame energy distribution of proton–L_α-photon pairs, as well as determine the specific set of molecular states excited in the collision. Furthermore, these excited molecular states resulting in the dissociation of the excited H_2^+ that produce a near-zero energy H^+ and a L_α photon are consistent with the results of a previous investigation that have used a different experimental technique [3].

Consider the characteristic total proton laboratory energy spectrum measured by Jaecks *et al.*, as shown in Fig. 1 [3]. Their experiment provided evidence for a previously unreported mechanism in the production of near-zero energy projectile frame protons in low kilo-electron-volt H_2^+-He collisions. By energy analyzing the protons produced in 4.0-keV H_2^+-He collisions in which the internuclear axis of H_2^+ was parallel to the beam axis, they found that the dominant process for the production of near-zero energy projectile frame protons is the $1s\sigma_g$ to $2p\pi_u$ and $3d\sigma_g$ transition at 2.5–3 times the equilibrium separation of H_2^+. These two states are shown in the H_2^+ potential-energy diagram of Fig. 2.

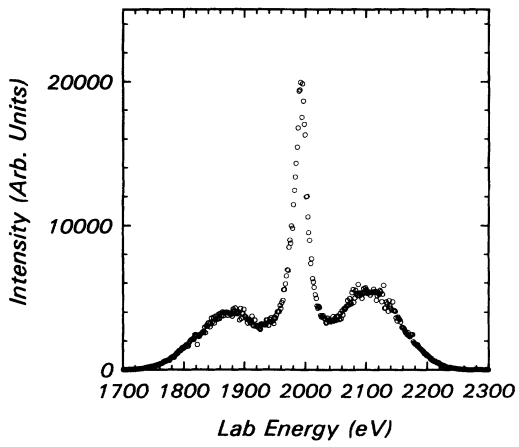

FIG. 1. Total laboratory energy spectrum of protons which are collected along the beam axis and produced in 4.0-keV H_2^+-He collisions (from Jaecks *et al.*) [3].

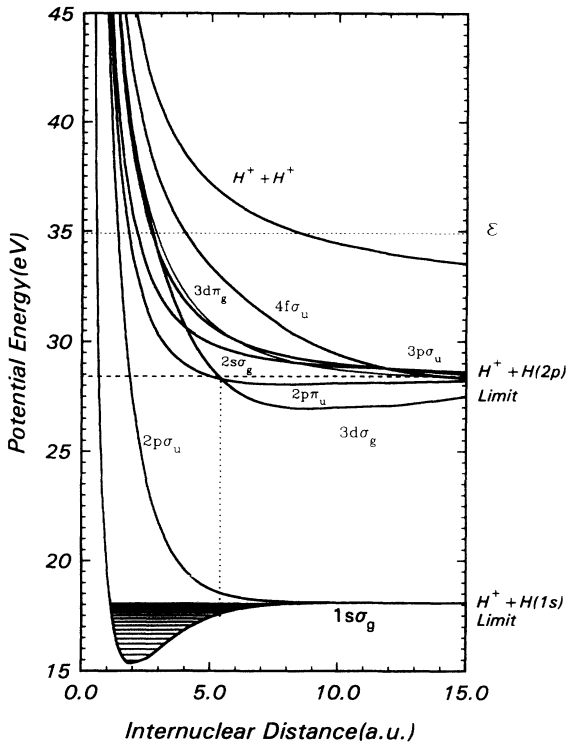

FIG. 2. H_2^+ energy curves leading to $H^+ + H$ ($n=2$). The vertical transition from the $1s\sigma_g$ to $2p\pi_u$ and $3d\sigma_g$ states is depicted by the dotted line. Processes producing transitions above the $H^+ + H$ ($n=2$) dissociation limit yield fragments with projectile frame energies $\epsilon_+ = \epsilon/2$. Note the number of states that can contribute to a particular ϵ. This gives a range of Q's and ϵ's such that $\Delta Q = \Delta\epsilon$. The ground vibrational states are also shown. Data for the plots are obtained from Bates, Ledsham, and Stewart [5] and Madsen and Peek [6].

The laboratory energy of each point in the spectrum can be described in the following manner. A Newton diagram representing the dissociation kinematics of H_2^+ via direct excitation is shown in Fig. 3. Since typical collision times are smaller than vibrational, rotational, and dissociation times, the molecule can be thought of as dissociating in two steps: excitation with subsequent dissociation. Assuming no center-of-mass deflection of H_2^+, the laboratory energy of the fragment proton in Fig. 1 can be readily written as

$$E_1 = \frac{E_0 - Q}{2} + \epsilon_+ + 2\left[\frac{(E_0 - Q)\epsilon_+}{2}\right]^{1/2} \cos\phi_1 , \quad (1)$$

where E_0 is the initial energy of H_2^+; Q the total inelastic energy lost during the collision, ϵ_+ the projectile frame kinetic energy imparted to the fragment particle, and ϕ_1 the instantaneous orientation of the parent molecule relative to the initial beam direction. It was shown in Ref. [3] that if center-of-mass deflection of H_2^+ occurs during the collision, the error in the determination of Q for direct excitation processes would be about 0.5 eV for a worst-case H_2^+ center-of-mass deflection of 0.5°. Thus the assumption of no c.m. deflection produces an error less than 0.5 eV in the determination of Q.

Since our experiment only measures protons produced along the beam axis, the sign on the last term of Eq. (1) reflects whether the proton is emitted in the forward or backward direction in the projectile frame. Protons with appreciable projectile frame velocities in the forward and backward directions relative to the incident-beam direction are represented by the broad, smaller peaks on either side of the central peak, and are known as Aston bands. The central peak represents protons of near-zero energy in the projectile frame. Since the detector solid angle for these protons is comparatively large, they appear as a dominant feature in the laboratory spectrum, though not a dominant process in the dissociation of H_2^+. Since $\epsilon_+ \approx 0$, these protons do not produce a distinct forward/backward peak structure, and Eq. (1) reduces to $E_1 = (E_0 - Q)/2$ for the central peak.

The total inelastic energy loss Q in Eq. (1) is comprised of the energy difference between the molecule's internal energy before and after the collision, the total energy needed to excite the target, and the recoil energy of the target. However, the latter quantity was shown to be negligible in determining Q for this collision process [3]. As evident from Fig. 2, both Q and ϵ_+ can occur over a distribution of inelastic energy losses and center-of-mass energies, since transitions may occur at different internuclear separation and from various initial vibrational levels of H_2^+. This gives rise to a range of Q's and ϵ_+'s such that $\Delta Q = 2\Delta\epsilon_+ = \Delta\epsilon$. By measuring the position of the central peak in Fig. 1, Jaecks *et al.* determined the inelastic energy loss Q at the main peak to be 11.6 ± 1.0 eV [3].

II. EXPERIMENT, PROCEDURE, AND RESULTS

The apparatus used for the measurement of the $H^+ - L_\alpha$-photon coincidences, as shown in Fig. 4, is the same as that used for the total proton laboratory energy distribution measurement [3]. The H_2^+ is formed in a duoplasmatron source. After extraction, acceleration, and momentum analysis, the collimated H_2^+ beam trav-

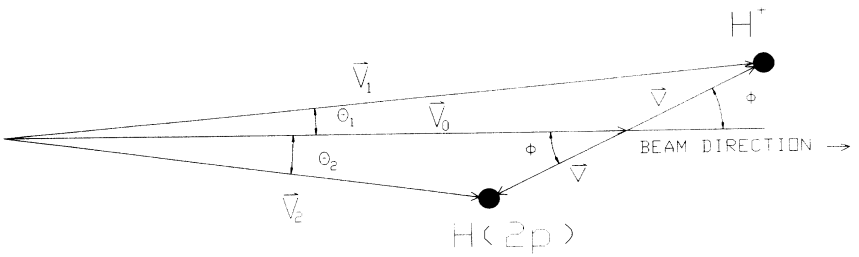

FIG. 3. Newton diagram depicting H_2^+ dissociation kinematics. The deflection of H_2^+ is neglected. See text for explanation.

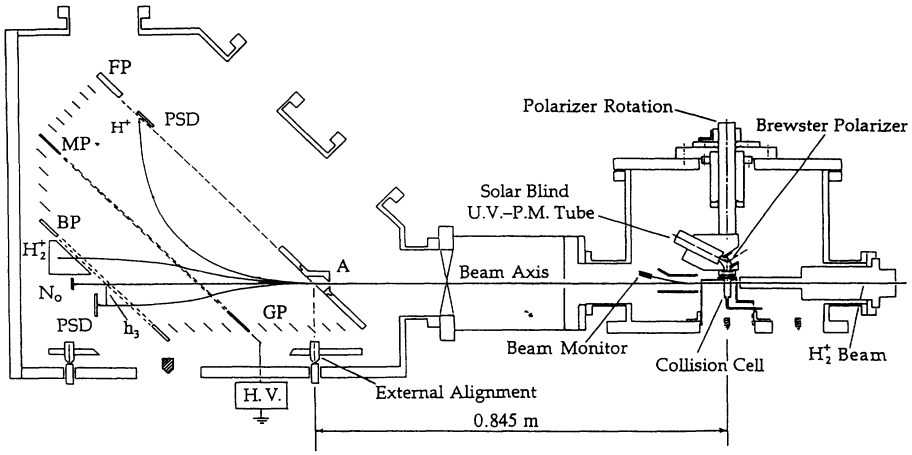

FIG. 4. Cross-sectional view of the experimental apparatus. Abbreviations are as follows: FP, front plate; MP, middle plate; BP, back place; PSD, position-sensitive detection; H.V., high voltage; GP, guard plate; A, aperture; U.V.-P.M. Tube, ultraviolet photomultiplier tube.

els through a differentially pumped collision cell where pressures are low enough to insure single collision interactions. Fragment protons are energy analyzed by a 45° two-stage parallel-plate energy analyzer [4], and protons are detected by a pair of microchannel plates (MCP's) in the chevron configuration. When a proton hits the front of this detector configuration, an avalanche of electrons are produced and are emitted from the back of the MCP's. These electrons hit a discrete Cu anode that is 1.5 mm in diameter, which corresponds to a laboratory acceptance angle of $\pm 0.024°$. The electronic pulse is then amplified and counted.

The polarized L_α photons which are also produced in the interaction region are analyzed by a LiF Brewster angle polarizer that is perpendicular to the plane defined by the incoming H_2^+ and the outgoing proton momenta vectors. The polarization axis of the LiF Brewster angle polarizer is kept at 45° with respect to the beam axis throughout the entire experiment. At this setting, the measured intensity is directly proportional to the total intensity of radiation emitted from the fragment, H(2*p*).

For each analyzer voltage setting V_{an}, pulses from the MCP's and the solar-blind photomultiplier tube (PMT) are amplified, discriminated, shaped, appropriately delayed, and fed into a time-to-amplitude converter (TAC). Since photon counts rates for the present experiment are about 60 Hz and the accompanying particle counts rates are in the kilohertz range, the signal from the PMT is used as the "start" input on the TAC. Output pulses from the TAC are fed into a multichannel analyzer (MCA) which collects the time spectrum. At the end of a run, the time spectrum is transferred to a computer for analysis. To reduce statistical error, the time spectrum for each analyzer voltage setting is collected several times. Average data accumulation time for each time spectrum is approximately 24 h at energies near the central peak of total proton energy distribution of Fig. 1, and increases to a maximum of 122 h at the largest laboratory energy. From each time spectrum, the number of true coincidences is determined and plotted. The laboratory energy spectrum of the coincident proton–L_α-photon pairs is displayed in Fig. 5. We have used a cubic spline interpolation to the data to guide the eye. These are represented by the continuous lines.

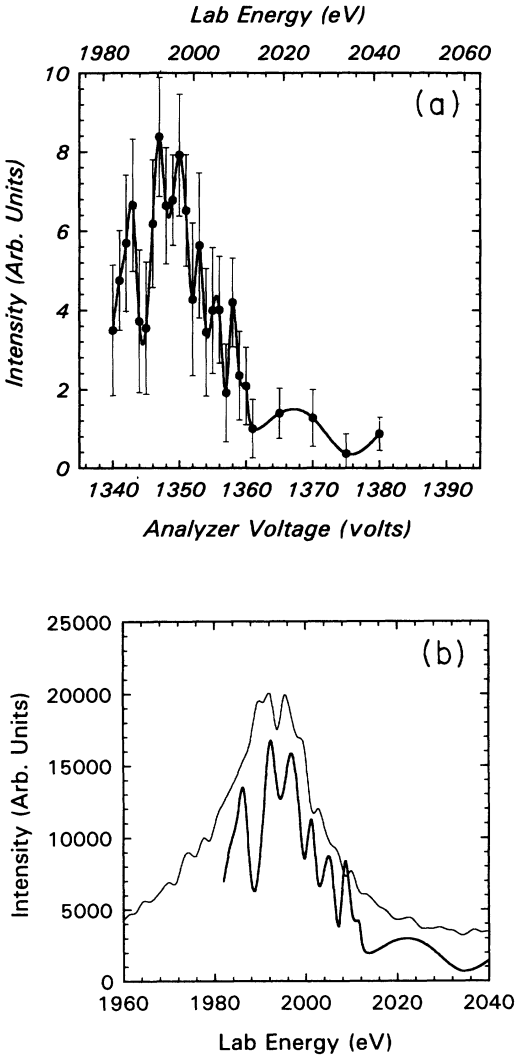

FIG. 5. (a) Laboratory energy distribution of H^+ detected along the beam axis in delayed coincidence with L_α photons. The L_α-photon polarization axis is set to 45° to the beam. (b) The laboratory spectrum of 5(a) (darker line) is superposed over the central peak of the proton's total laboratory energy spectrum of Fig. 1 (lighter line). Note the striking similarities in their structures.

Each data point is normalized to the total number of photons detected in each coincidence run, and represents a weighted average of several measurements. Assuming Poisson statistics, the error on each data point varies from 25 to 50%. Since typical proton counts are $\sim 10^9$ for each run, the normalization process introduces a statistical error $\sim 10^{-3}\%$ to each of the data points in Fig. 5. Since this contribution is very small, it is neglected in the statistical analysis.

III. DISCUSSION

Transformation of proton–L_α-photon laboratory energy spectrum

The coincidence data of Fig. 5(a) show a large peak that coincides with the near-zero energy projectile frame protons. Figure 5(b) shows an expanded version of the central peak of the total proton laboratory energy distribution of Fig. 1. It is interesting to note that peaks of both spectra have essentially the same features. Because of significant scatter in Fig. 5(a), it is difficult to find the centroid of the peak, and thus to determine a precise Q. However, if this spectrum is transformed into the projectile frame, then it is possible to obtain an estimate of the range of Q's producing the coincidence peak. This requires one to correct for the energy dependence of the detector's solid angle, constant in the laboratory frame, but changing in the projectile frame. In addition, we must take into account the changing energy resolution of the analyzer.

For an isotropic distribution of particles, the number of particles reaching the detector is directly related to the solid angle subtended by the detector. If the solid angle of the detector is constant for particles of different energies, then the energy distribution obtained from the detector reflects the actual distribution of energies. If, however, the detector solid angle is changing with energy, then the energy distribution acquired from this detector will reflect the energy dependence of the solid angle as well as the actual energy distribution.

The definition of the solid angle is

$$\Omega = \int \int \sin(\phi_1) d\phi_1 d\psi = \frac{A}{r^2} , \tag{2}$$

where ϕ_1 and ψ, respectively, are the polar and azimuthal angles of a spherical coordinate system, and A is the area on a sphere of radius r that is encompassed by the solid angle Ω. Using Fig. 6, ϕ_1 can be related to E_1, ϵ_+, and the laboratory scattering angle θ_1 through

$$\sin\phi_1 = \left[\frac{E_1}{\epsilon} \right]^{1/2} \sin\theta_1 . \tag{3}$$

To apply Eq. (2) to the analyzer, we project the anode of a detector onto the plane perpendicular to the beamline at the analyzer entrance slit. Our definition of anode projection requires that if we apply a voltage V_{an} to the analyzer so that we obtain particles of laboratory energy E_1 at this detector, then the particles of laboratory energy E_1 must pass through this projected area to reach the detector. The position and size of the projected anode will depend on the analyzer voltage, the laboratory energy of the particle, the location of the detector, and the smallest resolvable area on the detector.

The following calculation of the projectile frame solid angle is limited to detectors mounted at $\theta_1 = 0°$. Figure 6 shows an exaggerated view of the anode's projected area A' on the entrance slit's plane, and the spatial extent of an isotropic distribution of particles with the same velocity of the center of mass $\mathbf{V}_0$ and center-of-mass speed v. The center of the circle shown is the position of the c.m. when a proton emitted parallel to the beam direction enters the slit. The laboratory solid angle Ω_E seen by the detector is

$$\Omega_E \approx \frac{A'}{L_0^2} , \tag{4a}$$

while the center-of-mass solid angle is

$$\Omega_\epsilon \approx \frac{A'}{r^2} . \tag{4b}$$

The expression for the solid angle is no longer exact since we have used the flat projected area A' instead of the spherical area A. This approximation is good for small scattering angle ϕ_1, where the deviation of A' from A is small enough to be neglected. Since the present system has a detector anode with an approximately circular projected area of radius 0.5 mm, and a collision center to

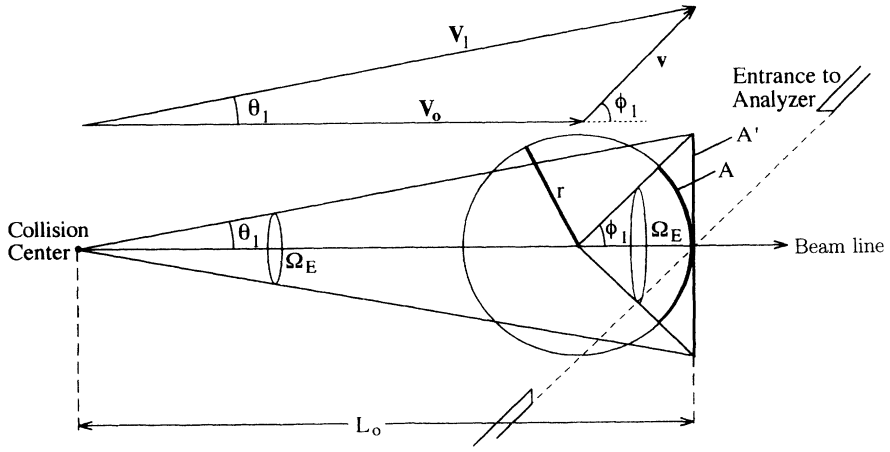

FIG. 6. Geometry for the solid angle calculation. It illustrates an exaggerated view of the projected area A' of the detector anode onto the plane perpendicular to the beamline at the entrance slit of the analyzer. Also shown is the spatial extent of the isotropic distribution of particles with the same velocity of center of mass V_0 and projectile frame speed v.

analyzer entrance slit distance of $L_0=33.25''$, we require that ϵ_+/E_1 be greater than 2.2×10^{-5} to incur less than 1% error in the solid angle.

The size of the projected area A' has a negligible energy dependence. Consequently, the laboratory solid angle Ω_E detected also remains constant since L_0 is constant. However, the projectile frame radius r, shown in Fig. 6, is energy dependent and indicates how the projectile frame solid angle is changing with energy. For the particle passing through the center of the projected area A', we can relate the projectile frame radius r shown in Fig. 6 to the fragment particle's laboratory frame speed and parent molecule's projectile frame speed through

$$r=L_0\left[\frac{V_1-V_0}{V_1}\right]=L_0\left\{1-\left[\left[\frac{E_0-Q}{2}\right]\frac{1}{E_1}\right]^{1/2}\right\}$$
$$=L_0(1-\xi)\ , \tag{5a}$$

where

$$\xi=\left[\frac{E_0-Q}{2E_1}\right]^{1/2}\ . \tag{5b}$$

Thus, the center-of-mass frame solid angle subtended by the projected detector area is

$$\Omega_\epsilon=\frac{A'}{L_0^2(1-\xi)^2}\ . \tag{6}$$

For any given detector, the relative energy resolution of the parallel-plate, electrostatic energy analyzer $\Delta E_1/E_1$ is constant. As we look at higher-energy particles, the range of ΔE_1 accepted by the detector increases. Consequently, we must consider the range of projectile frame energies accepted by the detector. If we write ϵ_+ as a function of the inelastic energy loss Q, and if we know the distribution of Q's, we can include its contribution to the spread in projectile frame energy. From Fig. 3, $\mathbf{v}=\mathbf{V}_1-\mathbf{V}_0$ and ϵ_+ is related to Q by

$$\epsilon_+=\frac{E_0-Q}{2}+E_1-2\cos\theta_1\left[\frac{E_0-Q}{2}E_1\right]^{1/2}\ . \tag{7}$$

The general expression for the spread in projectile frame energies of the protons is

$$\Delta\epsilon_+=\frac{\partial\epsilon_+}{\partial E_1}\Delta E_1+\frac{\partial\epsilon_+}{\partial Q}\Delta Q+\frac{\partial\epsilon_+}{\partial E_0}\Delta E_0+\frac{\partial\epsilon_+}{\partial\theta_1}\Delta\theta_1$$
$$=(1-\xi)\Delta E_1+\frac{(\xi-1)}{\xi}\frac{(\Delta E_0-\Delta Q)}{2}\ . \tag{8}$$

Note that the contributions due to the uncertainty in θ_1 is zero for this specific case, since the $\Delta\theta_1$ term of Eq. (8) contains a factor that is proportional to $\sin\theta_1$.

Using the relationship $\Delta Q=2\Delta\epsilon_+$ and solving for $\Delta\epsilon_+$, one obtains

$$\Delta\epsilon_+=\frac{(2\xi\Delta E_1-\Delta E_0)(1-\xi)}{2(2\xi-1)} \tag{9}$$

for the dissociation of H_2^+. For the present measurement, the energy resolution of the analyzer is $\Delta E_1/E_1=0.33\%$. The quantity ΔE_0 refers to the uncertainty in the initial energy of the projectile, and has been estimated to be about 10 eV.

Using Eqs. (6) and (9), and the laboratory frame proton spectrum of Fig. 5(a), we can deduce the distribution of protons in the projectile frame. Assuming that the distribution of particles of energy ϵ_+ is isotropic in the projectile frame, the number of particles $N(V_{an})$ detected in a given time interval, at an analyzer voltage V_{an}, is given by

$$N(V_{an})=N_{c.m.}(\epsilon_+)\frac{\Omega_\epsilon}{4\pi}\Delta\epsilon_+\Gamma \tag{10}$$

where $N_{c.m.}(\epsilon_+)$ is the total number of particles produced with projectile frame energy ϵ_+, in the given time interval; Ω_ϵ the projectile frame solid angle subtended by the detector; Γ the detector efficiency, assumed to be energy independent; and $\Delta\epsilon_+$ the range of proton energies accepted by the detector, over which $N_{c.m.}(\epsilon_+)$ is assumed to be constant. Combining Eq. (10) with Eqs. (9) and (6) and solving for $N_{c.m.}(\epsilon_+)$, we find

$$N_{c.m.}(\epsilon)\approx N(V_{an})\frac{2(2\xi-1)(1-\xi)}{(2\xi\Delta E_1-\Delta E_o)}\left[\frac{4\pi L_0^2}{\Gamma A'}\right]\ . \tag{11}$$

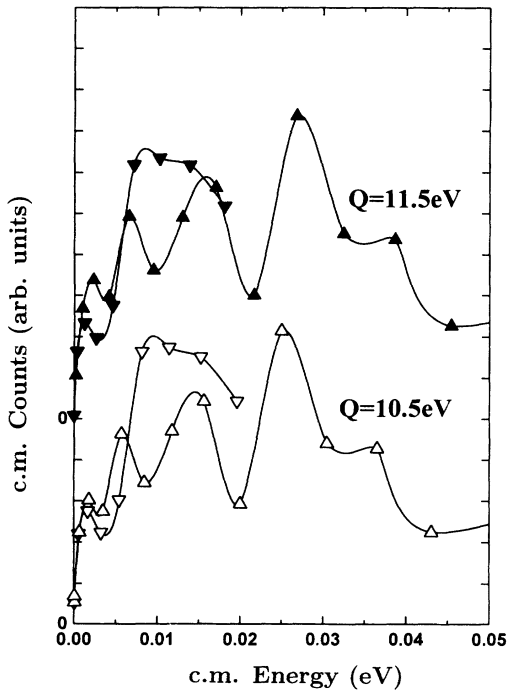

FIG. 7. Projectile frame distribution of coincident H^+-L_α-photon pairs. The triangles represent protons emitted in the forward direction. The inverted triangles show protons emitted in the opposite direction with respect to the initial beam. Filled triangles correspond to an inelastic energy loss of $Q=11.5$ eV, and unfilled ones to $Q=10.5$ eV. Cubic spline interpolations of the data are used to guide the eye. These are represented by the continuous lines. The range of Q values for which the emitted forward and backward protons are symmetric about $\epsilon_+=0$ was determined to be 11 ± 1 eV.

Note that the rightmost term in parentheses contains only constants. When transforming a laboratory energy spectrum, each data point will be scaled by this same constant, and we can ignore it without altering the structure of Eq. (10). By varying the parameter Q, we find a range of values of the inelastic energy loss for which the emitted forward and backward protons are symmetric about $\epsilon_+ = 0$.

Using Eq. (11) and the data of Fig. 5(a), we obtain a projectile frame distribution of the coincident proton–L_α-photon pairs. The results of the transformation for two Q values are shown in Fig. 7. Again, we have used cubic spline interpolations to the data to guide the eye. These are represented by the continuous lines. We find the approximate inelastic energy loss for the coincidence spectrum of Fig. 5 to be 11 ± 1 eV. This value is in good agreement with the previous results of Jaecks *et al.*; using a different technique Q was found to be 11.6 ± 1.0 eV [3]. Thus, using two separate methods, we have shown that the production of near-zero energy projectile frame protons for this process is due to transitions from $1s\sigma_g$ to $2p\pi_u$ and $3d\sigma_g$ at 2.5–3 times the equilibrium separation of H_2^+.

IV. CONCLUSION

We have measured the laboratory energy distribution of coincident proton–L_α-photon pairs produced in 4.0-keV H_2^+-He collisions. After transforming these data into the projectile frame, from the symmetry of the forward- and backward-emitted protons with negligible velocities in the projectile frame, we have determined an approximate energy loss of $Q = 11\pm1$ eV for the production of near-zero energy protons in coincidence with L_α photons. This value is in excellent agreement with earlier measurements of Jaecks *et al.* [3], who determined a Q of 11.6 ± 1 eV, using a separate experimental method. Our results suggest that the dominant process for producing near-zero energy projectile frame energy protons is the $1s\sigma_g$ to $2p\pi_u$ and $3d\sigma_g$ transition at 2.5–3 times the equilibrium separation of H_2^+, which reinforces the conclusions of Jaecks *et al.*[3]. The transformation of the laboratory energy distribution of coincident proton–L_α-photon pairs into the projectile frame has provided an elegant method of deconvoluting the manifold processes contained in its spectrum.

ACKNOWLEDGMENT

The support of this work by the National Science Foundation, under Grant No. PHY-9120213, is gratefully acknowledged.

[1] U. Fano and W. Lichten, Phys. Rev. Lett. **14**, 627 (1965); M. Barat and W. Lichten, Phys. Rev. A **6**, 2311 (1972).
[2] D. H. Jaecks, O. Yenen, M. Natajaran, and D. Mueller, Phys. Rev. Lett. **50**, 825 (1983).
[3] D. H. Jaecks, O. Yenen, L. M. Wiese, and D. Calabrese, Phys. Rev. A **41**, 5934 (1990).
[4] D. Calabrese, O. Yenen, L. M. Wiese, and D. H. Jaecks, Rev. Sci. Instrum. **65**, 116 (1994).
[5] D. R. Bates, K. Ledsham, and A. L. Stewart, Philos. Trans. R. Soc. London, Ser. A **246**, 215 (1953).
[6] M. M. Madsen and J. M. Peek, At. Data **2**, 171 (1971).